Mitochondrial DNA-Activated cGAS-STING Signaling in Environmental Dry Eye

Xiying Tan, Qianqian Chen, Zhonghua Chen, Zhenzhen Sun, Wei Chen, and Ruifen Wei

State Key Laboratory of Ophthalmology, Optometry and Vision Science, Eye Hospital, Wenzhou Medical University, Wenzhou, Zhejiang, China

Correspondence: Ruifen Wei, State Key Laboratory of Ophthalmology, Optometry and Vision Science, Eye Hospital, Wenzhou Medical University, 270 West Xueyuan Road, Wenzhou, Zhejiang 325027, China; weiruifen@eye.ac.cn.
Wei Chen, State Key Laboratory of Ophthalmology, Optometry and Vision Science, Eye Hospital, Wenzhou Medical University, 270 West Xueyuan Road, Wenzhou, Zhejiang 325027, China; chenweimd@wmu.edu.cn.

WC and RW contributed equally to this work.

Received: September 26, 2023
Accepted: March 17, 2024
Published: April 22, 2024

Citation: Tan X, Chen Q, Chen Z, Sun Z, Chen W, Wei R. Mitochondrial DNA-activated cGAS-STING signaling in environmental dry eye. *Invest Ophthalmol Vis Sci.* 2024;65(4):33. https://doi.org/10.1167/iovs.65.4.33

Purpose. The cGAS-STING pathway has been shown to be an important mediator of inflammation. There is emerging evidence of the importance of this signaling cascade in a variety of inflammatory diseases settings. Here, we present evidence that the mitochondrial DNA (mtDNA) damage-mediated cGAS-STING pathway plays an important role in the induction of inflammation in environmental dry eye (DE).

Methods. RT-qPCR and Western blot were used to assess the induction of the cGAS-STING pathway and inflammatory cytokines in environmental DE mouse model, primary human corneal epithelial cells (pHCECs), and patients with DE. RNA sequencing was used to determine mRNA expression patterns of high osmotic pressure (HOP)–stimulated pHCECs. mtDNA was detected with electron microscopy, flow cytometry, and immunofluorescent staining. mtDNA was isolated and transfected into pHCECs for evaluating the activation of the cGAS-STING pathway.

Results. The expression levels of cGAS, STING, TBK1, IRF3, and IFNβ were significantly increased in an environmental DE model and HOP-stimulated pHCECs. The STING inhibitor decreased the expression of inflammatory factors in DE. An upregulation of STING-mediated immune responses and IRF3 expression mediated by TBK1 were observed in the HOP group. HOP stimulation induced mitochondrial oxidative damage and the leakage of mtDNA into the cytoplasm. Then, mtDNA activated the cGAS-STING pathway and induced intracytoplasmic STING translocated to the Golgi apparatus. Finally, we also found activated cGAS-STING signaling in the human conjunctival blot cell of patients with DE.

Conclusions. Our findings suggest that the cGAS-STING pathway is activated by recognizing cytoplasmic mtDNA leading to STING translocation, further exacerbating the development of inflammation in environmental DE.

Keywords: dry eye, cGAS-STING pathway, mitochondrial DNA, inflammation

Dry eye (DE) is a multifactorial syndrome that has millions of patients seeking treatment at outpatient clinics annually.[1,2] Due to the drastic changes in the living environment, environmental stresses, including the popularity of video display terminals and air conditioning, as well as deterioration of the daily environment, have become the major risk factors of DE in this new era.[3,4] Therefore, environmental DE catches more and more researchers' attention. Pathologic changes of environmental DE also include an increase in tear osmolarity and the development of ocular surface inflammation. Many studies over the past two decades have provided a better understanding of the inflammation in environmental DE, being both a triggering factor and one of the key mechanisms that contributes to the development of environmental DE.[5,6] During this process, numerous inflammatory cytokines and chemokines are released into the cornea and conjunctival epithelium.[7,8] The major mediators have been shown to be IL-6, IL-17A, IL-1β, TNF-α, and MMP9. In addition, studies have shown that acute dryness and mitochondrial oxidative damage in DE activate stress signaling pathways in the corneal epithelium and residential immune cells.[9,10] This, in turn, activates innate immune responses and triggers the production of innate inflammatory mediators. All of this contributes to tear film instability and worsening of symptoms, leading to the formation of a vicious circle.

A recent study showed that mitochondrial fragmentation and autophagy activation plays a significant role in the pathogenesis of DE.[11] It has also been demonstrated that oxidative damage to mitochondrial DNA (mtDNA) can disrupt the homeostasis of inflammatory vesicles, which promotes DE.[12] However, few studies have examined the role of mitochondrial damage in the pathogenesis of dry eye. Mitochondria are highly immunogenic organelles,[13] as damaged and dysfunctional mitochondria release damage-associated molecular patterns, that induce inflammatory responses by triggering immune activation via pattern-recognition receptors in both immune and nonimmune cells.[14,15] Furthermore, it has been shown that mtDNAs are detected via pathogen-associated molecular patterns (PAMPs) being recognized as aberrant DNA.[16–18] PAMPs include three major receptors: toll-like receptor 9, melanoma

immunodeficiency factor 2, and cyclic guanosine adenosine monophosphate synthetase (cGAS), which leads to the activation of stimulator of interferon genes (STING).[19] The cGAS-STING pathway is a major intracytoplasmic DNA recognition signaling pathway in mammalian cells. Numerous studies have shown that mtDNA can be directly recognized by intracytoplasmic cGAS and activate the cGAS-STING pathway in inflammatory diseases and antitumor responses.[20–23]

STING signaling is associated with the endoplasmic reticulum (ER).[24] cGAS captures foreign or self double-stranded DNAs (dsDNAs, including nuclear and mtDNAs) entering the cytoplasm[25] and stimulates STING, causing STING to migrate from the ER to the Golgi apparatus and ultimately to localize in perinuclear endosomes. Here, it assembles with TBK1 leading to the activation of two inflammatory pathways in the nucleus and the production of type I interferons.[26,27] This pathway significantly contributes to the host defense by activation of the innate immune system.[24] Recent studies have identified a close link between the cGAS-STING pathway and the development of several inflammatory diseases[28–32] and a potential new therapeutic target.[33] There are several studies showing the role of the cGAS-STING pathway in keratitis and age-related macular degeneration.[34–37] Recently, a report proposed the hypothesis that dsDNA, as well as the cGAS-STING pathway, could play an important role in the pathogenesis of DE.[38] Since then, the cGAS-STING pathway has been demonstrated as a key mediator of ocular surface inflammation in two nonenvironmental experimental DE models, a chemical treated model and a surgically intervened model. The cGAS-STING pathway is the sensor of innate immune system, whereas environmental conditions can affect the innate immune system directly. However, in environmental DE, it is still unknown whether the cGAS-STING pathway is activated. Herein, we conducted a series of experiments to evaluate the functional mechanisms of the cGAS-STING pathway in environmental DE.

In this study, we uncovered that mitochondrial damage generates aberrant mtDNA that activates the cGAS-STING pathway, which promotes the development of inflammation and significantly contributes to the pathogenesis of environmental DE. Also, the application of the STING inhibitor can alleviate the ocular inflammation in environmental DE, which may provide additional therapeutic targets for the development of new treatments for environmental DE.

Materials and Methods

Mouse Environmental DE Model

Six- to 8-week-old female C57BL/6 mice were provided by the Experimental Center of Wenzhou Medical University and approved by the Experimental Animal Ethics Committee of Wenzhou Medical University. Mice were exposed to low-humidity conditions in our proprietary intelligent control environmental system (ICES) to induce environmental DE under these conditions for 2 weeks.[39] The control group was housed with humidity of 60% to 80%, no airflow, and temperature of 22 ± 2°C. The DE group was housed in chambers maintained at a humidity of 13.1% ± 3.5%, airflow of 2.2 ± 0.2 m/s, and temperature of 22 ± 2°C. At the end of this period, corneal epithelial cells and conjunctiva were harvested and preserved in RNA lysis buffer or protein lysis buffer.

Evaluation of Sodium Fluorescein Staining in Mice

On days 0 and 14, mice were evaluated by slit-lamp examination and sodium fluorescein staining. To stain mouse corneas, 0.5 µL sodium fluorescein solution (1 mg of sodium fluorescein was dissolved in 0.5 mL of 0.9% physiologic saline) was applied to the conjunctival sacs of both eyes. Observations were made with a cobalt blue light using a slit-lamp microscope 2 minutes after staining. The National Eye Institute Standard Classification was chosen as the scoring criteria: the mouse cornea was divided into five regions: superior, inferior, nasal, temporal and central, and the staining of each region was scored 0 to 3 (0 points, no punctate staining; 1 point, scattered punctate staining; 2 points, diffuse punctate staining; 3 points, lamellar staining). The five regional scores were added together for a total score of corneal fluorescein staining. Each examination was performed by the same researcher and conducted in a single-blind manner.

Real-Time PCR

Total RNA was extracted from harvested cells with RNA lysis buffer (RLT; Applied Biosystems, Grand Island, NY, USA) and 0.2 mg RNA from each sample was reverse transcribed with M-MLV reverse transcriptase (Applied Biosystems) according to the manufacturer's instructions. The gene sequences are listed in Supplementary Table S1.

Immunoblotting

Protein was extracted using an ice-cold lysis buffer and ultrasonic dispersion. The suspension was centrifuged at 15,000 rpm for 15 minutes, and the supernatant protein concentration was determined using the BCA assay. Samples containing 10 µg protein were subjected to SDS-PAGE and then transferred to polyvinylidene difluoride membranes (Roche, Basel, Switzerland). Membranes were blocked with fat-free milk and then probed overnight with primary *cGAS* (31659S; Cell Signaling Technology, Danvers, MA, USA, 1:500), *STING* (13647S; Cell Signaling Technology; 1:3000), *TBK1//NAK* (3013S; Cell Signaling Technology; 1:500), *Phospho-TBK1//NAK* (5483S; Cell Signaling Technology; 1:500), *IRF-3* (4302S; Cell Signaling Technology; 1:500), *Phospho-IRF-3* (29047S; Cell Signaling Technology; 1:500), or GAPDH (5174S; Cell Signaling Technology; 1:3000). This was followed by incubating with horseradish peroxidase–conjugated goat anti-rabbit IgG (Bioworld Technology, Nanjing, China; 1:5000). Blots were developed with an ECL detection system (Pierce Biotechnology, Rockford, IL, USA). GAPDH was used as a loading control.

Cell Culture

Primary human corneal epithelial cells (pHCECs) were cultured from fresh human corneoscleral tissues acquired from the Eye Bank of Wenzhou. Tissues were dissected into several pieces and cultured in a supplemented hormonal epidermal medium (SHEM) with 5% fetal bovine serum (FBS). After several days, corneal epithelial cells grew out of the corneal limbus. Cells were maintained in a humidified 5% CO_2 incubator at 37°C, and culture medium was changed every other day. High osmotic pressure (HOP) group cells were cultured in 450 osmotic pressure media (mOsm) by adding 85 mM sodium chloride to media and

Investigative Ophthalmology & Visual Science

incubated 2 hours for quantitative PCR (qPCR) and 24 hours for Western blotting. As a control, human corneal epithelial cells (HCECs) were cultured under normal osmotic pressure (310 mOsm). Confluent corneal epithelial cultures were then cultured with SHEM with H151 (*STING* inhibitor; Selleck, Houston, Texas, USA) or SHEM with 0.1% DMSO (Beyotime, Shanghai, China). After being treated for 2 hours, protein or total RNA from pHCECs was extracted.

Immunostaining

HCECs were plated on 12-well plates (Corning, Corning, NY, USA) in complete medium at 37°C with 5% CO_2. Cells were fixed with 4% paraformaldehyde for 30 minutes at room temperature, blocked in 10% serum at 37°C for 30 minutes, and finally incubated with the clone *AE-2* antibody (32160702; Sigma, Darmstadt, Germany; 1:100), *TOM20* monoclonal antibody (66777-1-IG; Thermo Fisher Scientific, Rockford, IL, USA), anti-Calnexin (AF18) (sc-23954; Santa Cruz Biotechnology, Santa Cruz, CALI, USA), anti-GM130 (B-10) (sc-55591; Santa Cruz Biotechnology, Santa Cruz, CALI, USA), and anti–ER-Golgi intermediate compartment (ERGIC) 53 (C-6) (sc-365158; Santa Cruz Biotechnology, Santa Cruz, CALI, USA) at 4°C overnight. Cells were then incubated with a species-matched Alexa Fluor 488–conjugated secondary antibody (Thermo Fisher Scientific; 1:200), Alexa Fluor 594–conjugated secondary antibody (Thermo Fisher Scientific; 1:200), and DAPI (Beyotime Biotechnology; 1:1000) for 15 minutes in the dark at room temperature. In addition, stained cells processed without primary antibodies served as negative controls. Cells were visualized and imaged using a fluorescence microscope (Zeiss LSM 880; Zeiss, Kyoto, Japan).

CM-H2DCFDA Assay to Detect Intracellular Reactive Oxygen Species

pHCECs were cultured in 96-well black/clear-bottom plates. Wells were seeded with 1.5×10^4 cell, and each plate was divided into two groups. Each group had three duplicate plates. Test groups were stimulated for 2 hours, then washed with PBS. After PBS aspiration, 100 µL CM-H2DCFDA working fluid (5 µM/mL, diluted in PBS) was added to each well. The plate was incubated at 37°C in the dark for 30 minutes. Cells were then washed with PBS three times, and 100 µL PBS with 1% FBS was added to each well. The cells were immediately imaged with an inverted fluorescence microscope.

mtDNA Extraction and Transfection

mtDNA from pHCECs was extracted using a Mitochondrial DNA Isolation Kit (ab65321; Abcam, Cambridge, MA, USA) according to the kit protocol. Briefly, approximately $5 \times g$ pHCECs were homogenized with 1 × Cytosol Extraction Buffer and transferred to a 1.5-mL tube and centrifuged at $600 \times g$ for 10 minutes at 4°C. The supernatant was transferred to a new 1.5-mL tube and centrifuged at $10{,}000 \times g$ for 30 minutes at 4°C. After centrifugation, the supernatant and precipitates were solubilized by adding mitochondrial isolation buffer (30 µL), followed by the addition of the enzyme mix (5 µL), and lightly mixed. This mixture was then incubated in a water bath at 50°C for 60 minutes. The mtDNA was precipitated by centrifugation at room temperature at maximum speed for 5 minutes. The mtDNA was lysed and the DNA concentration was measured using a NanoDrop 2000 spectrophotometer (Thermo Fisher Scientific).

The Attractene Transfection Reagent (301,005, Qiagen, Duesseldorf, Germany) was used to induce mtDNA transfection into pHCECs according to the kit protocol. The extracted mtDNA was first mixed with serum and antibiotic-free cell culture medium to 100 µL and then mixed by adding Attractene Transfection Reagent (4.5 µL), followed by centrifugation of the homogenate and standing at room temperature for 15 minutes to form the transfection complex. After pHCECs, cultured under normal conditions (37°C and 5% CO_2), had reached 70% confluence, the medium was replaced with new complete medium and the transfection complex was applied to the cells and incubated for 4 hours. HCEC cells were incubated for 3 hours before the medium was changed and was incubated for 3 additional hours after application of the transfection complex.

qPCR to Determine the mtDNA Copy Number in the Cytoplasm

The pHCEC mitochondria were extracted using the Mitochondria Isolation Kit for Cultured Cells (C3601; Beyotime) according to the kit protocol. Approximately 5×10^6 pHCECs were collected. Cells were resuspended in 250 µL of mitochondrial isolation reagent and incubated for 15 minutes on ice. The cell suspension was homogenized at a low temperature using a Dounce cell grinder, and the homogenate was transferred to a 1.5-mL tube before centrifuging at $600 \times g$ for 10 minutes at 4°C. The supernatant was transferred to a new tube and centrifuged at $11{,}000 \times g$ for 10 minutes at 4°C. The supernatant (now cytoplasm) was transferred to a new 1.5-mL tube.

The DNA within the cytoplasm was then isolated using the FlexiGene DNA Kit (No. 51206; Qiagen). Briefly, 300 µL FG1 was added to the collected cytoplasm and mixed well before the addition of 300 µL FG2 and inverted three times. The homogenate was incubated in a 65°C water bath for 10 minutes before the addition of 600 µL of 100% isopropanol to induce the precipitation of DNA. The precipitate was then centrifuged at $10{,}000 \times g$ for 3 minutes. The supernatant was discarded and 200 µL FG3 was added and incubated at 65°C for 30 minutes to dissolve the DNA.

After obtaining the cytoplasmic DNA solution, the intracytoplasmic mtDNA copy number was detected using RT-qPCR. The mtDNA using primers that bind to the gene encoding mitochrome c oxidase 1 (mt-Co1) and nuclear DNA using primers that bind to the gene encoding 18S rDNA (encoding 18S rRNA) were used. Cytoplasmic mtDNA copy number levels were compared between the two groups using nuclear DNA as the baseline. All primers were synthesized by Tsingke Biological Technology (Shanghai, China). The *mt-Co1* primer sequence is 5′-GCCCCCGATATGGCGTTT-3′ (forward) and 5′-GTTCAACCTGTTCCTGCTCC-3′ (reverse). The *18S rDNA* primer sequence is 5′-TAGAGGGACAAGTGGCGTT-C-3′ (forward) and 5′-CGCTGAGCCAGTCAGTGT-3′ (reverse).

Chemical Enzyme Labeling Apparatus to Detect Intracellular ATP Concentration

The intracellular ATP was detected using the ATP Detection Kit (S0026; Beyotime) according to the kit protocol.

The culture medium was aspirated and the cells were lysed by adding lysate at the ratio of 200 µL of lysate per well of a 6-well plate. After lysis, the cells were centrifuged at 12,000 × *g* at 4°C for 5 minutes, and the supernatant for the subsequent assay removed. The reagents to be used were melted on an ice bath, and the ATP standard solution was diluted with ATP assay lysate to the appropriate concentration gradient. The appropriate amount of ATP Assay Working Solution was prepared at a ratio of 100 µL ATP Assay Working Solution per sample or standard. The reagents to be used were melted in an ice bath. The appropriate amount of ATP Assay Reagent was taken and the ATP Assay Reagent with ATP Assay Reagent Diluent was diluted at a ratio of 1:9. Then, 100 µL ATP Assay Working Solution was added to the assay well or tube and allowed to stand at room temperature for 3 to 5 minutes to allow all of the background ATP to be consumed. Then, 20 µL of sample or standard was added to the assay wells or tubes and mixed quickly with a micropipette, and the RLU value by chemiluminescence was measured (SpectraMax 190; Molecular Devices, SanDiego, California, USA) after a minimum interval of 2 seconds. Finally, the concentration of ATP in the sample was calculated from the standard curve.

Flow Cytometry

MitoSOX Red Mitochondrial Superoxide Indicator (M36008; Thermo Fisher Scientific) was used to detect superoxide levels within pHCECs. A 5-µM MitoSOX working solution was prepared and 1 mL of working solution was added to the harvested pHCECs and incubated for 10 minutes at 37C° in the dark. Cells were washed three times with PBS, and the difference in cell fluorescence intensity between the two experimental groups was determined using a flow cytometer (Invitrogen Attune NxT V6; Thermo Fisher Scientific).

Changes in the mitochondrial membrane potential of pHCECs induced by hyperosmolarity were detected using JC-1 dye (Mitochondrial Membrane Potential Probe) (T3168; Thermo Fisher Scientific). A 2-µM JC-1 dye working solution was prepared and the harvested pHCECs were resuspended in 1 mL of working solution and incubated for 30 minutes at 37°C in the dark. Cells were washed three times with PBS and then examined by flow cytometry (Invitrogen Attune NxT V6; Thermo Fisher Scientific) to determine the differences in cell fluorescence intensity and fractionation percentages between the two experimental groups.

Electron Microscopy

pHCECs fixed with glutaraldehyde were rinsed three times with 0.1 M phosphate buffer (pH 7.2) for 15 minutes each. Cells were then fixed in 1% starvation acid/0.1 M phosphate buffer (pH 7.2) for 2 hours at room temperature and rinsed three times with 0.1 M phosphate buffer (pH 7.2) for 15 minutes each. Cells were dehydrated by 30%, 50%, 70%, 80%, 85%, 90%, 95%, and 100% (twice) alcohol gradients for 15 to 20 minutes each. Cells were permeabilized using acetone/epoxy resin (2:1), acetone/epoxy resin (1:1), and epoxy resin for 8 to 12 hours in a 37°C incubator. The cells were placed in an embedding plate, and embedding agent epoxy resin was added and polymerized for 48 hours at 60°C. The samples were sliced into 80- to 100-nm slices using an ultrathin slicer (EM UC7; Leica, Heidelberg, Baden-Württemberg, Germany). After uranium-lead double staining (2% uranyl acetate saturated in water, lead citrate, 15 minutes at room temperature), sections were dried at room temperature overnight and observed by electron microscopy (TEM Hitachi HT7650; Hitachi, Tokyo, Japan).

Patient Selection

All procedures involving human participants adhered to the principles of the Declaration of Helsinki and were approved by the Institutional Research Ethics Committee (2022-138-K-107-01) of the Eye Hospital of Wenzhou Medical University. Written informed consent was obtained from all patients prior to participation in the study. The diagnosis of environmentally induced DE follows the "New Perspectives on Dry Eye Classification: Recommendations from ADES," published in *Eye and Contact Lens* in 2020.[40] Inclusion criteria include complaints of DE-related symptoms, no topical anti-inflammatory medication other than artificial tears, Ocular Surface Disease Index (OSDI) >13 points, tear film breakup time (TBUT) <5 seconds, or noninvasivce break up time (NIBUT) <10 seconds. Patients with a history of eye disease other than DE, eye surgery, contact lens use, any systemic medication, and pregnancy were excluded. Normal participants with no DE symptoms, OSDI <13, and TBUT >5 seconds were included. The right eye was selected for statistical analysis.

Human Conjunctival Impression Cytology

One drop of proparacaine hydrochloride eye drops (s.a. ALCON-COUVREUR n.v., Bruxelles, Belgium) was used to temporarily anesthetize the participant's ocular surface. A 3 × 3 × 4.5-mm (right trapezoidal) polyethersulfone membrane (SuporPall Gellman Science, East Hills, NY, USA) was placed on the globular conjunctiva for 10 seconds. The membrane was placed in 350 µL RNA lysis buffer (RLT; ABI, NY, USA) to obtain human conjunctival blot cell sample and stored at −80°C until isolation.

Statistical Analysis

RNA sequencing data were analyzed using R 4.1.1 (R Foundation for Statistical Computing, Vienna, Austria) software. $P < 0.05$ was considered statistically significant. Data were graphed using GraphPad Prism 6 software (GraphPad Software, San Diego, CA, USA) and SPSS 19.0 (IBM Corporation, Armonk, NY, USA). Statistical analysis was performed using one-way ANOVA followed by a Tukey's test. All values are expressed as mean ± SD, and values of $P < 0.05$ were considered statistically significant.

Results

The cGAS-STING Pathway Is Activated in Corneal Epithelial Tissue of Environmental DE

In vivo studies, after 2 weeks of ICES exposure, we observed that the fluorescein staining score was significantly higher compared with the control group and was obviously lower after the treatment of STING inhibitor H151 in the DE group (Fig. 1A, $P < 0.001$). The protein levels of cGAS, STING, P-TBK1, TBK1, P-IRF3, and IRF3 were differentially increased (Fig. 1B). Additionally, the mRNA expression levels

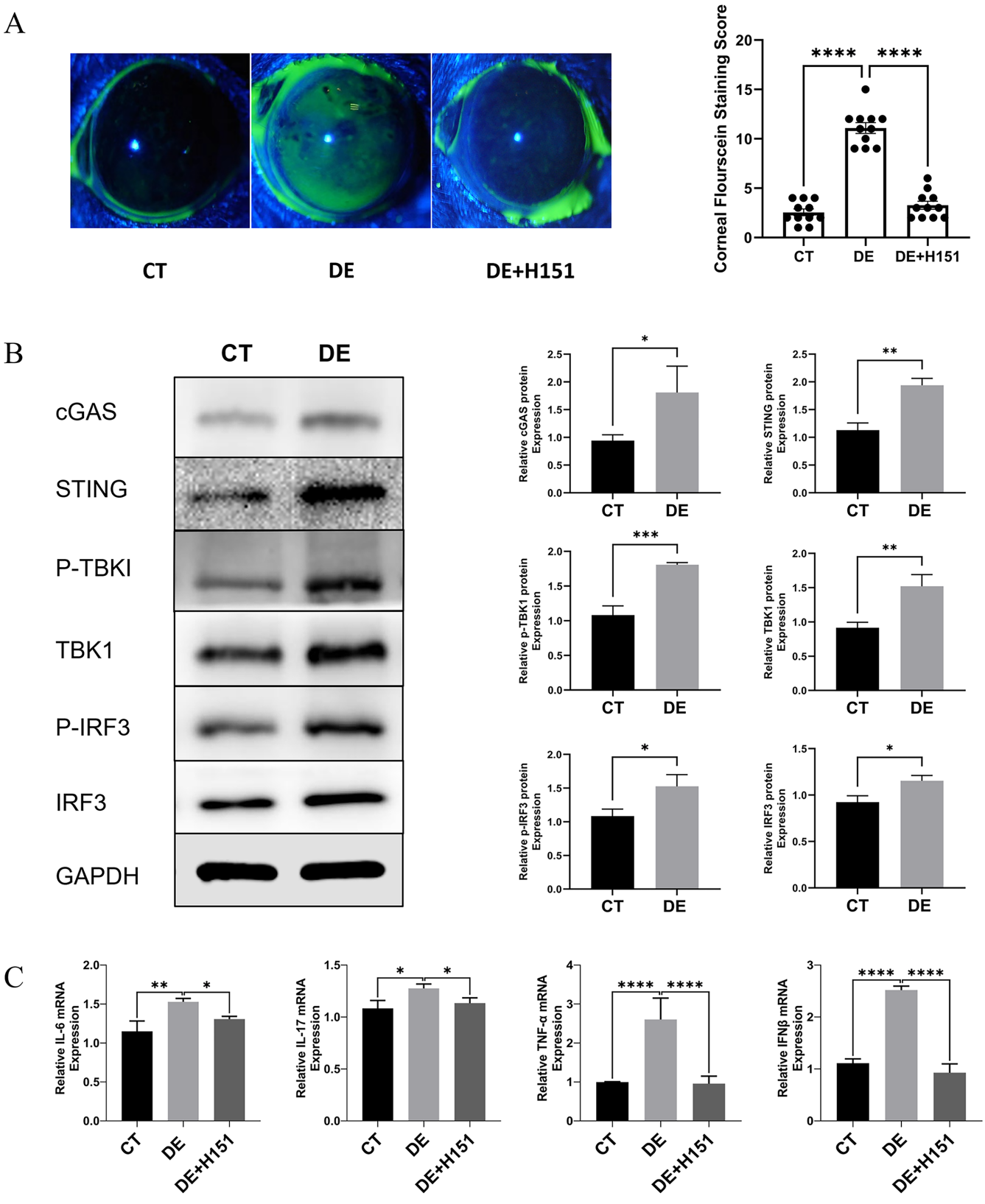

Figure 1. Increased activation of the cGAS-STING pathway in a corneal epithelium in murine DE model. (**A**) Representative corneal staining images and score of the control (CT), DE, and H151 treated group (n = 11/group). (**B**) Western blot results of protein expression levels of the cGAS-STING pathway in the corneal epithelium (n = 3/group). (**C**) RT-qPCR results of the expression of inflammatory factors in the corneal epithelial tissues of the CT, DE, and DE + H151 group (n = 6/group). The data are presented as mean ± SD. *P < 0.05, **P < 0.01, ***P < 0.001, ****P < 0.0001. Protein expression levels are quantified by densitometry for protein plots.

Investigative Ophthalmology & Visual Science

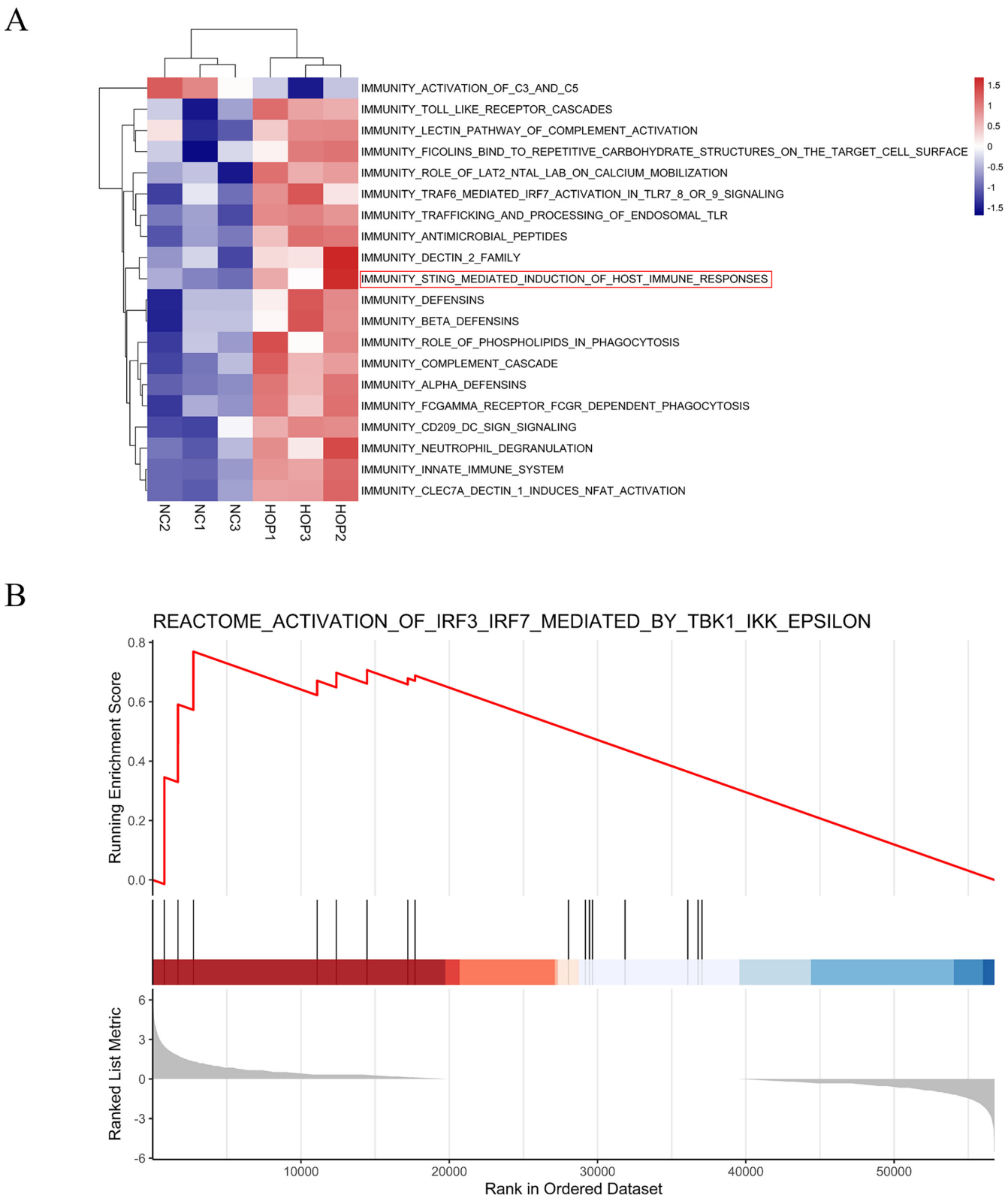

Figure 2. Hyperosmotic stress enhances STING-mediated immune responses in pHCECs. (**A**) Top 20 most significantly changed pathways in single-sample gene set enrichment analysis (sGSEA) in the DE group (n = 3/group). (**B**) Gene set enrichment analysis (GSEA) shows TBK1-mediated activation of IRF3 in pHCECs under osmotic stress. A distinct peak (*red line*) denoting a strong positive correlation among the highest-ranked genes. The middle portion's color gradient represents gene regulation, with *red* indicating upregulated genes and *blue* indicating downregulated ones in response to the stress. *Black vertical bars* represent the position of each member in the target gene set.

Investigative Ophthalmology & Visual Science

of IL-6, IL-17A, TNF-α, and IFN-β in corneal epithelial tissues were significantly increased in the DE group (Fig. 1C). To further investigate the role of the cGAS-STING pathway in DE, we topically treated mice with the STING inhibitor H151 during the 2 weeks of DE induction. The results show a significant reduction in the expression of IL-6, IL-17A, TNF-α, and IFN-β in the DE group after treatment with H151 compared to the untreated group (Fig. 1C).

Hyperosmolarity Increases STING-Mediated Immune Responses in pHCECs

We performed a single-sample gene set enrichment analysis in R 4.1.1 (R Foundation for Statistical Computing) using the innate immune system–related pathway from the Reactome database (https://reactome.org/) on primary epithelial cells after hyperosmotic stress. The top 20 pathways with the most significant changes ($P < 0.05$) are shown (Fig. 2A), including upregulation of the STING-mediated induction of the host immune responses pathway, which is underlined with a red box. Red represents high expression, which is in contrast to the low expression (blue). In addition, a simultaneous gene set enrichment analysis of the innate immune system–related pathways in the Reactome database showed upregulated activation of IRF3 mediated by TBK1 epsilon (Fig. 2B). The vertical axis represents a gene enrichment, which shows increased enrichment of genes in the *IRF3-TBK1* gene axis in the cells associated with HCECs under osmotic stress.

Hypertonicity Induces Activation of the cGAS-STING Pathway and Inhibitors Downregulate Inflammatory Expression in pHCECs

A significant increase in protein expression of the cGAS-STING pathway-related factors was observed (Figs. 3A, 3B). To further investigate the role of the cGAS-STING pathway in DE, we used the STING inhibitor H151 to inhibit the expression of STING in pHCECs. RT-qPCR assays showed that treatment with H151 inhibited the activation of the cGAS-STING pathway and inflammatory factors in DE (Fig. 3C).

Hyperosmotic Stress Induces Mitochondrial Dysfunction in pHCECs

Examination by electron microscopy suggested significant changes in mitochondrial morphology with loss of mitochondrial cristae and rupture of the outer membrane in pHCECs after hyperosmotic stimulation (Fig. 4A). Flow cytometric analysis indicated that the proportion of cells stained with the JC-1 monomer stain increased significantly compared with those stained with the multimer stain, suggesting an increased number of cells with decreased mitochondrial membrane potential after hyperosmotic stimulation (Fig. 4B). After hypertonic stimulation of pHCEC for 2 hours, an enhancement of intracytoplasmic reactive oxygen species (ROS) fluorescence was observed by fluorescence staining compared with the normal group, indicating an increase in intracellular oxidative stress (Supplementary Fig. S1). These results also indicate a significant increase in fluorescence intensity via Mito-SOX staining after hyperosmotic stimulation compared with the control group (Fig. 4C), suggesting increased oxidative stress in the mitochondria. A decrease in intracellular ATP content was also observed after hyperosmotic stimulation (Fig. 4D).

Hypertonicity Induces Leakage of mtDNA Into the Cytoplasm in pHCECs

Double-staining for intracytoplasmic dsDNA (clone AE-2) and mitochondria (TOM20 Monoclonal Antibody) was done to observe intracytoplasmic dsDNA and mtDNA (dsDNA colocalized with mitochondria) via immunofluorescence microscopy in pHCECs. As shown in Figure 5A, free intracytoplasmic dsDNA and mtDNA were substantially increased in pHCECs after hyperosmotic stimulation compared to the normal control (NC) group. In addition, the negative control group is shown in Supplementary Figure S2, which indirectly proves the specificity of staining with anti–AE-2 and anti-TOM20 antibodies. To confirm the leakage of intracytoplasmic mtDNA, we extracted intracytoplasmic DNA from pHCECs after hyperosmotic stimulation and directly detected the mtDNA copy number using RT-qPCR (based on primers designed for mtDNA sequences). These results showed a significant increase of intracytoplasmic mtDNA copy number after hyperosmotic stimulation (Fig. 5B).

mtDNA Activates the cGAS-STING Pathway in pHCECs and Promotes STING Translocation

We performed transfection stimulation experiments using mtDNA extracted from pHCECs cells. Protein expression level of cGAS was significantly increased after mtDNA transfection stimulation, and the downstream factors STING, TBK1, and IRF3 were significantly increased (Fig. 6A). The addition of H151 to mtDNA-transfected pHCECs led to a decrease in inflammatory factors associated with DE (Fig. 6B).

STING was diffusely distributed in the endoplasmic reticulum in the control group. In the mtDNA-transfected group (1 µg for 6 hours) and the HOP group, STING translocation occurred as movement was observed from the endoplasmic reticulum and partially accumulated on the ER–Golgi intermediate compartment (ERGIC) and the Golgi apparatus in the cytoplasm (Fig. 7). In addition, the negative control groups are shown in Supplementary Figure S3, which indirectly proves the specificity of staining with mentioned antibodies.

cGAS-STING Pathway Is Activated in Conjunctiva of an Environmental DE Murine Model

To comprehensively observe the changes in the ocular surface, we examined the induction of the cGAS-STING pathway in the conjunctiva of a DE murine model. The protein levels of cGAS, STING, TBK1, and IRF3 were significantly increased in the DE group compared to the control group (Supplementary Fig. S4).

cGAS-STING Pathway Expression Increases in Patients With DE

We recruited 11 DE participants (11 left eyes) and 11 normal participants (11 left eyes). There were no significant differences in gender and age between the two groups (Table). The DE group had a higher OSDI scores ($P < 0.0001$) and a much lower TBUT value ($P < 0.05$). RT-qPCR showed that

Investigative Ophthalmology & Visual Science

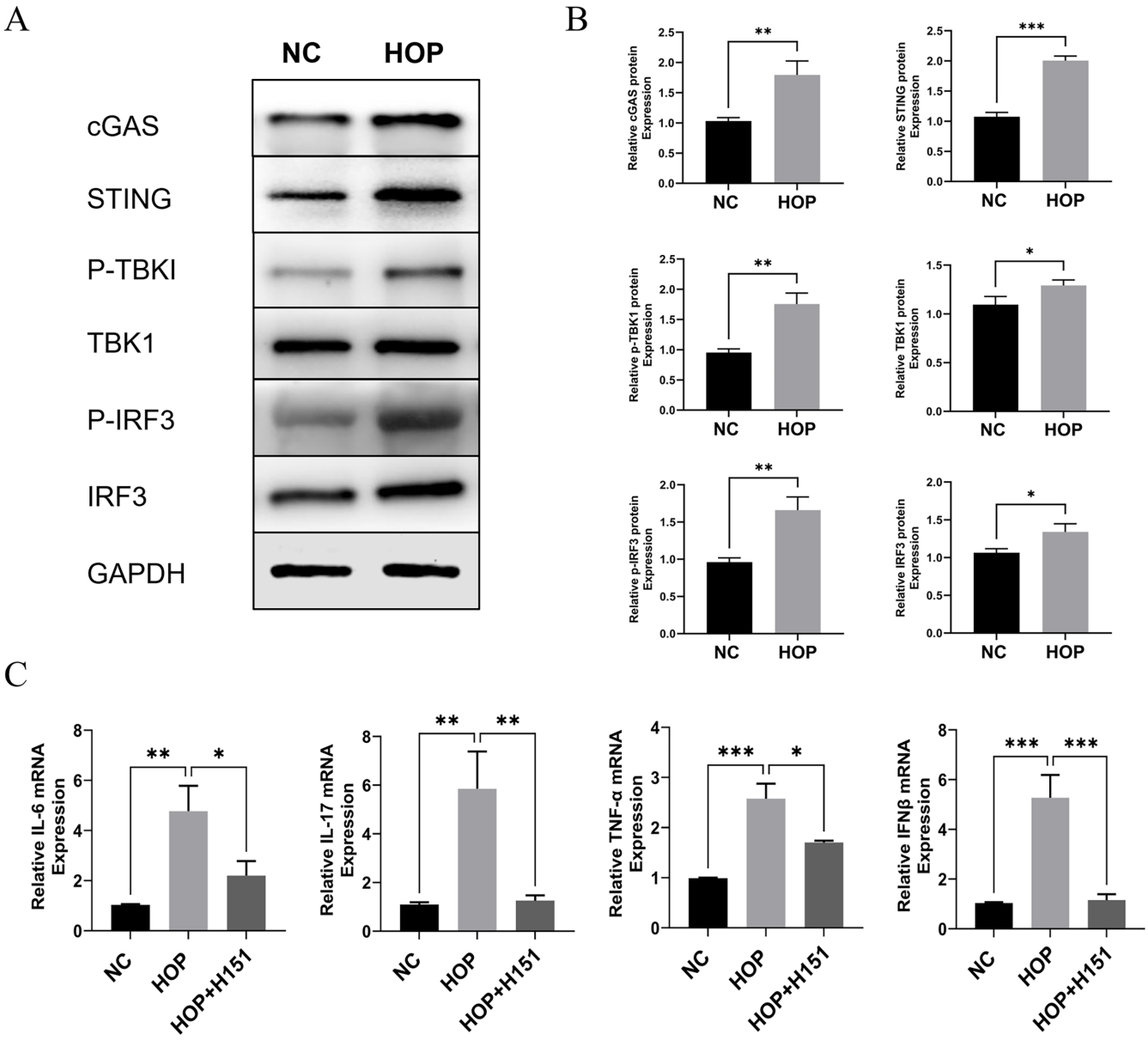

Figure 3. Hyperosmotic stress induces the activation of the cGAS-STING pathway in pHCECs. (**A**, **B**) Protein expression of cGAS, STING, P-TBK1, TBK1, P-IRF3, IRF3, and IFN-β in pHCECs of NC and HOP groups (n = 3/group). (**C**) Gene expression of inflammatory factors in NC, HOP, and HOP + H151 groups (n = 4/group). The data are presented as mean ± SD. *P < 0.05, **P < 0.01, ***P < 0.001. Protein expression levels are quantified by densitometry for protein plots.

the expression levels of cGAS, STING, TBK1, IRF3, and IFN-β were significantly higher in the human conjunctival blot cell sample of patients with DE (Fig. 8). This suggests that the cGAS-STING pathway is activated in patients with DE.

Discussion

Accumulating studies demonstrated that the abnormal innate immune response at the ocular surface induces DE,[5] whereas the innate immune system can be profoundly affected by environmental stresses. Importantly, the cGAS-STING pathway is a crucial component of the innate immune system. Thus, we assumed that the cGAS-STING pathway is the bridge between environmental stresses and DE. Interestingly, our data demonstrate an activation of the cGAS-STING pathway in patients with DE and an in vivo/vitro environmental DE model, which suggests a potential role of the cGAS-STING pathway in the pathogenesis of environmental DE. Notably, a recent study[38] found that the cGAS-STING pathway is activated in a chemical or surgically intervened DE model, but the role of cGAS-STING pathway in environmental DE is not clear. The biggest difference between our study and the abovementioned research is that we used the ICES mice model to better simulate the environmental factors that induce the DE. The ICES model is designed to well represent the environmental factors[39] that lead to excessive evaporation of tears, which is one of the most important causes in environmental DE; also, we used the pHCECs and the conjunctival cells from patients with DE to better reveal the role of the cGAS-STING pathway in environmental DE.

Investigative Ophthalmology & Visual Science

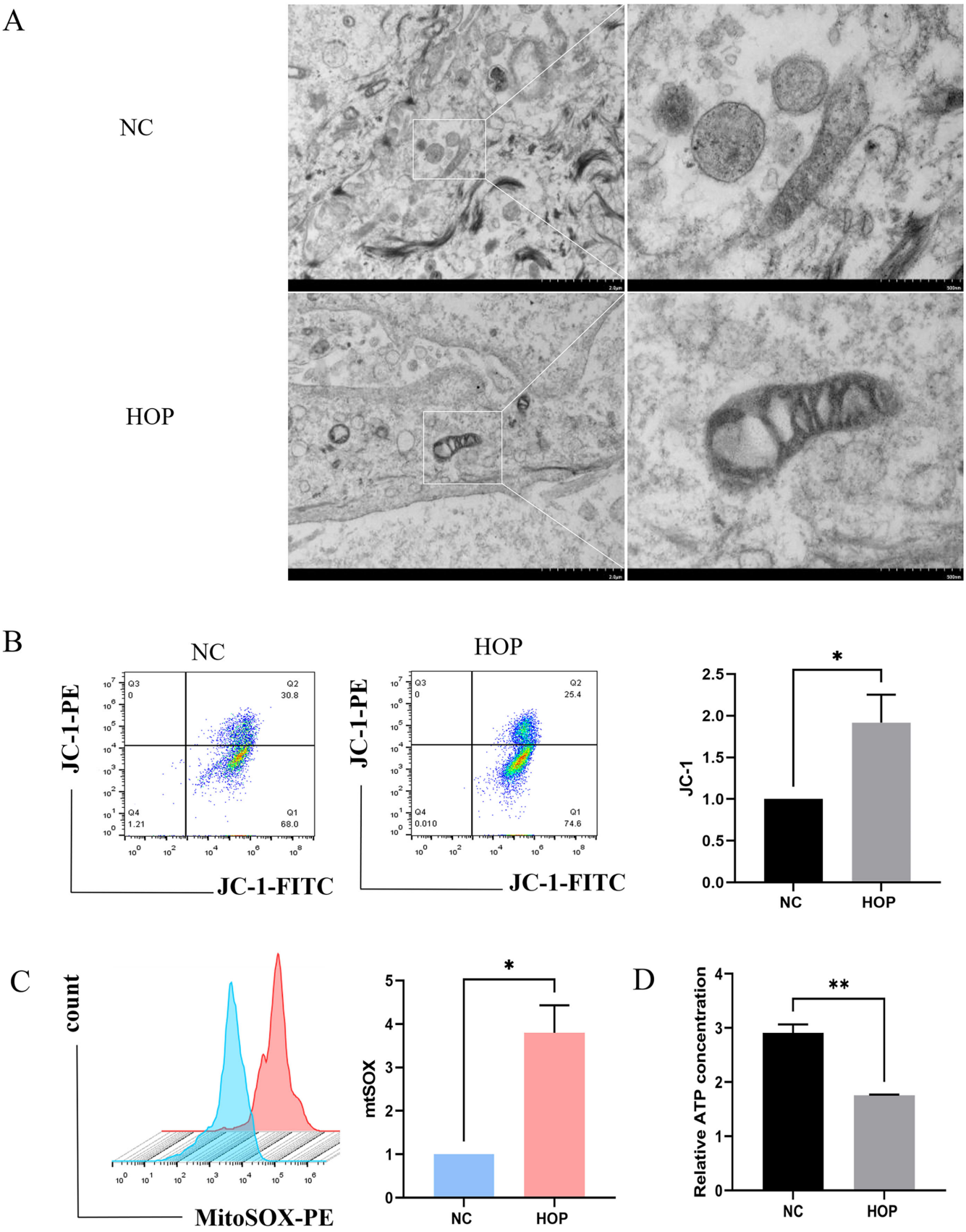

Figure 4. Hyperosmolarity induces mitochondrial dysfunction in pHCECs. (**A**) Electron microscopy was used to visualize the morphology of mitochondria within the cytoplasm of pHCECs after hyperosmotic stimulation. (**B**) Changes in mitochondrial membrane potential in mitochondria after JC-1 staining by flow cytometry. (**C**) Oxidative stress after MitoSOX staining by flow cytometry. (**D**) Changes in ATP levels within pHCECs after hypertonic stimulation detected by zymography (n = 6/group). The data are presented as mean ± SD. *P < 0.05, **P < 0.01.

Investigative Ophthalmology & Visual Science

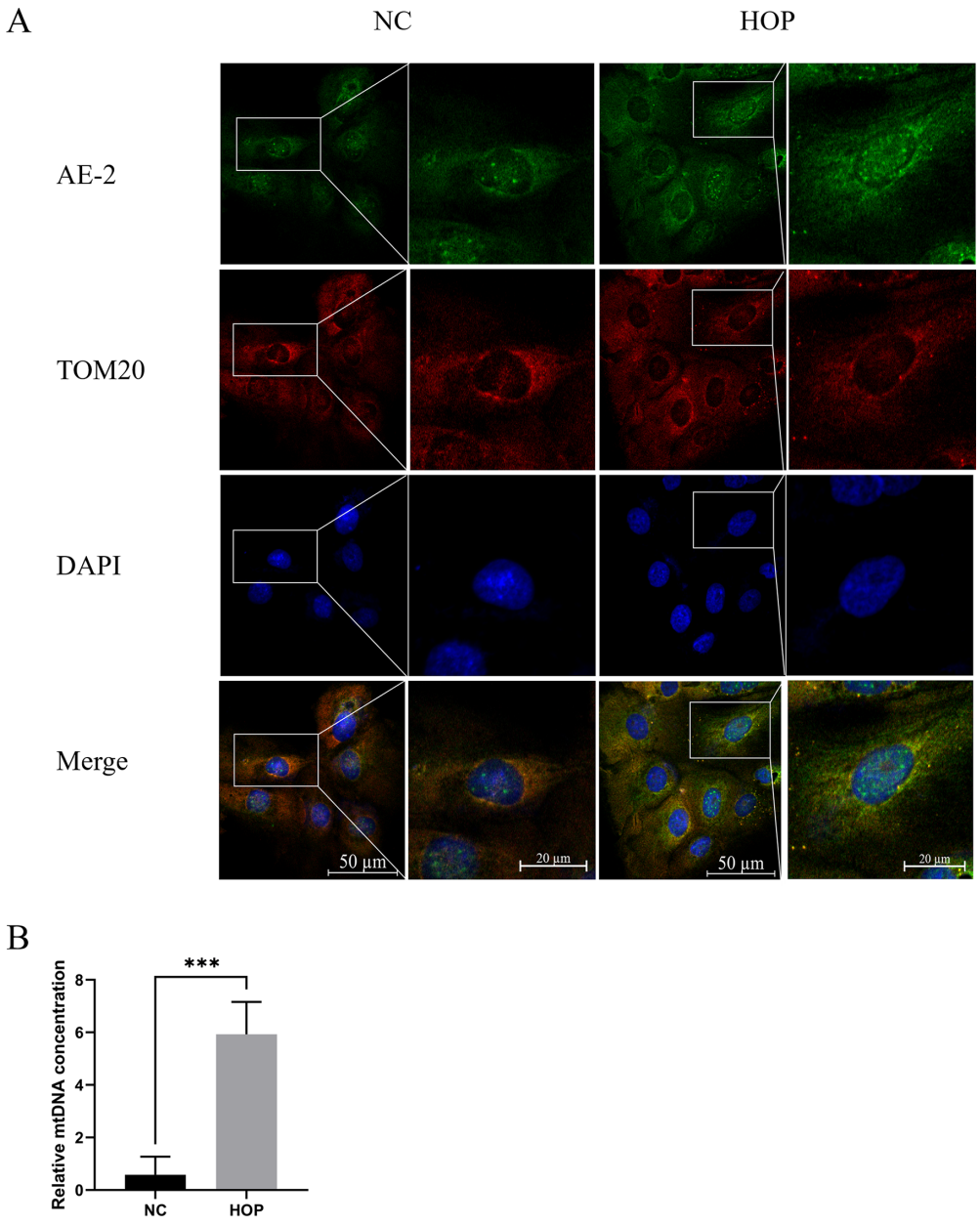

Figure 5. Hyperosmotic stress induces increased intracytoplasmic mtDNA of pHCECs. (**A**) Intracellular dsDNA, mitochondrial localization, and fluorescence intensity of pHCECs were observed via an immunofluorescence microscope. (**B**) Changes in mtDNA level of pHCECs in the hyperosmotic group detected by RT-PCR ($n = 6$/group). The data are presented as mean ± SD. ***$P < 0.001$.

Collectively, our study provides clear evidence for a possible contribution of cGAS-STING in the development of environmental DE.

Although the cGAS-STING pathway is essential for innate immune disorders, few other studies have been published regarding the role of the cGAS-STING pathway in ocular diseases. Previous studies have demonstrated that the cGAS-STING pathway activates the innate immune system in corneal infections with HSV-1.[36,37] In *Aspergillus fumigatus* keratitis, the cGAS-STING pathway is also involved in the promotion of the inflammatory response.[35] This evidence suggests that the cGAS-STING pathway has a significant role in the disease process that occurs after corneal infections. Additional studies show that mtDNA activates the cGAS-STING pathway in retinal microvascular endothelial cells to drive atypical inflammation,[41] and subsequent in vivo experiments by this research group confirm the intracellular cytoplasmic mtDNA activation of cGAS-STING, which induces retinal dysfunction,[42] suggesting that the cGAS-STING pathway participates in molecular mechanisms of pathogenesis that are associated with the inflammatory response in the eye. In systemic diseases, many studies report a close link between the cGAS-STING pathway and the pathologic mechanisms of inflammatory diseases. Patients with systemic lupus erythematosus have elevated levels of cGAMP, and this can be reversed by STING knockdown in mice with a lupus-like phenotype.[43–45] In rheumatoid arthritis, it has been proposed that cytokine expression is decreased following knockdown of either cGAS or STING.[46] As inflammation is central to the pathogenesis of DE, these studies are consis-

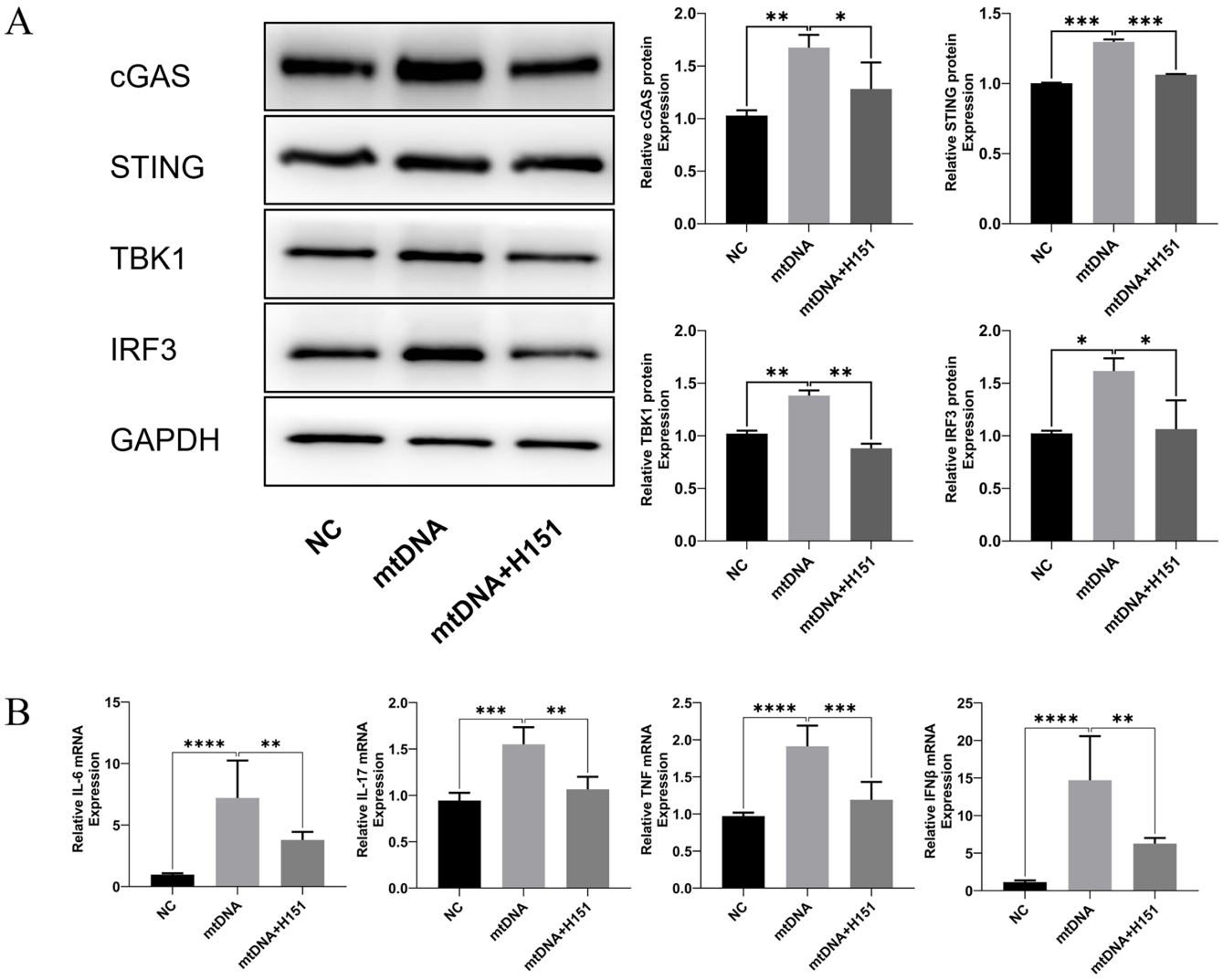

Figure 6. mtDNA activates the cGAS-STING pathway in pHCECs. (**A**) Protein expression levels of cGAS, STING, TBK1, and IRF3 (n = 3/group). (**B**) Gene expression of inflammatory factors stimulated by mtDNA transfection followed by treatment with H151 (n = 3/group). The data are presented as mean ± SD. *P < 0.05, **P < 0.01, and ***P < 0.001. Protein expression levels are quantified by densitometry for protein plots.

tent with our data showing the activation of the cGAS-STING pathway is a crucial process in environmental DE.

Previously, our and other studies have revealed the importance of ROS in environmental DE.[47–49] Here we further show that exposure to high osmolarity induces excess ROS in the mitochondria of pHCECs, as well as impaired mitochondrial function and damaged mitochondrial morphology. But in the latest study,[38] the authors found the inhibiting mtDNA oxidation by exogenous 8-OHDG did not downregulate the cGAS-STING pathway, which shows that mtDNA oxidation is not the cause of cGAS-STING activation in the HCEC line. One reason might be due to other regulatory events leading to such results, so the mechanism of oxidative stress leading to DE needs further studies.

Additionally, we observed that excess mtDNA in the cytoplasm induced activation of the cGAS-STING pathway, resulting in the translocation of STING from the endoplasmic reticulum to the perinuclear endosomes in DE. This accumulation triggers the production of downstream inflammatory factors. mtDNA enters the cytoplasm by rupture or permeabilization of mitochondrial membranes after mitochondrial damage.[50] Alternatively, mtDNA may escape from mitochondria into the cytoplasm via the mitochondrial permeability transition pore (mPTP) in retinal microvascular endothelial cells.[41] Especially, in a latest study,[38] they revealed that HCEC mtDNA was released into the cytoplasm through the mPTP under hyperosmotic stimulation, which led to mtDNA leakage. Overall, these data suggested that mtDNA release is complex in DE.

The treatment efficiency of the STING inhibitor in environmental DE, which may be caused by cytoplasmic mtDNA, is not clearly verified. In this study, we report that STING inhibition reversed the increased expression of inflammatory factors in both a hyperosmolarity-induced cellular model and an in vivo model, suggesting that the cGAS-STING pathway may be a potential target for the treatment of DE. Recently, it has been shown that the BRD4 inhibitor JQ1 (which epigenetically regulates the inhibition of STING transcription) attenuated oxidative stress–induced retinal inflammation and degeneration, and it thus may

Investigative Ophthalmology & Visual Science

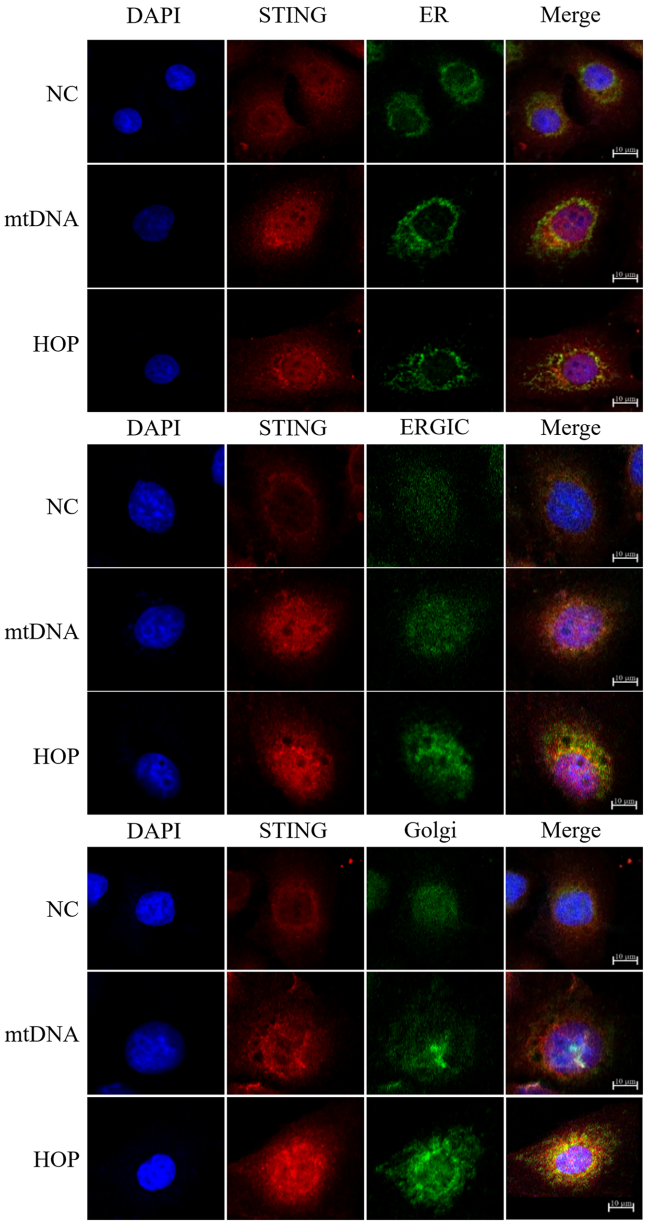

Figure 7. mtDNA promotes STING translocation in pHCECs. Colocalization of STING fluorescence localization with ER, ERGIC, and Golgi in the cytoplasm after stimulation by mtDNA transfection and HOP stimulation of pHCECs.

provide a potential therapeutic strategy for targeting the cGAS-STING pathway in age-related macular degeneration.[34] Similarly, our study provides a rationale for the targeting of the cGAS-STING pathway in the development of therapeutics for DE. In neoplastic diseases, the cGAS-STING signaling pathway has a central role in the immune response to tumors. cGAS-STING pathway activators have shown therapeutic efficacy in the treatment of tumor diseases,[51,52] and a number of clinical trials have been conducted to test potential biologic therapies.[53–56] To further investigate the potential application of the STING inhibitor in environmental DE treatment, we applied one kind of STING inhibitor, H151, in ICES mice, pHCECs, and mtDNA-transfected cells. We have demonstrated that inhibition of STING can alleviate the inflammation response, which is caused by mtDNA leakage. As a most widely used typical inhibitor of the cGAS-STING pathway, H151 effectively suppresses the expression of STING. H151 significantly dampens inflammatory signaling pathways in amyotrophic lateral sclerosis and human dental pulp tissue.[23,57] H151 has been shown to prevent IFN-β, TNF-α, and IL-6 production induced by DNA transfection in acute lung injury.[58] H151 can downregulate the expression levels of adhesion molecule and chemokines, accompanied by decreased adhesive ability and chemotaxis of immunocytes.[58] These studies are consistent with our results showing that H151 inhibits inflammation in DE. In the latest study,[38] they used one kind of STING inhibitor, C-176, in mice and also found its efficiency in alleviating the inflammation of the ocular surface in vivo. Thus, these studies together confirmed the importance of STING in mediating inflammation in DE.

Table. Demographics and Clinical Characteristics of NC and DE Patients. The data are presented as mean ± SD. ** $P < 0.01$, and *** $P < 0.001$.

Characteristic	NC	DE	*P* Value
Number of cases	11	11	—
Percentage of females	54.50	63.60	—
OSDI, mean ± SD	10.01 ± 1.548	38.09 ± 12.05	<0.001***
TBUT, mean ± SD	5.273 ± 2.240	2.909 ± 0.831	<0.01**

We next sought to ask how the cGAS-STING pathway exerts its effects in DE. There are two main downstream factors in the cGAS-STING pathway, including TBK1 and NF-κB.[24–26] To find out the main contributing factor, we did an RNA sequencing analysis of pHCECs, which is shown as the TBK1 pathway that contributes to building environmental DE. Our data suggest that the TBK1 pathway may play an important role as the application of H151 effectively dampens TBK1 expression, which provides evidence of the environmental DE treatment method. Ouyang et al.[38] also found the upregulation in the protein level of P-TBK1 in HCECs. Additional studies need to be conducted to examine the downstream role of NF-κB. The induction of autophagy has been shown to be a pivotal function in the activation of the cGAS-STING pathway as the strong activation of autophagy is a unique and important feature of the pathway.[59] Mitochondrial dysfunction and cytosolic mtDNA stress activate the cGAS-STING pathway, which triggers autophagy and promotes esophageal squamous cell carcinoma progression.[60] Moreover, activation of the cGAS-STING pathway in *A. fumigatus* keratitis has been reported to promote autophagy and inflammatory activation.[35] Accordingly, we speculate that autophagy may be a downstream target molecule of this pathway in the pathogenesis of DE. Interestingly, we observed a significant upregulation of IFN-β in the DE model. IFN-β is a major effector of the cGAS-STING pathway in the development of autoimmune diseases and inflammatory diseases. Type I IFN has been shown to have a significant role in the pathogenesis of Sjögren syndrome, but the exact mechanism remains unclear. A clinical study showed that type I IFN activation in neutrophils of patients with Sjögren syndrome led to mitochondrial damage and associated ROS production.[61] Since Sjögren syndrome is a major risk factor for the pathogenesis of DE, we hypothesized that IFN-β may play an important role as a downstream factor of the cGAS-STING pathway.

The study demonstrated that (1) the cGAS-STING pathway is highly expressed in environmental DE disease; (2) the cGAS-STING pathway is activated by recognition of mito-

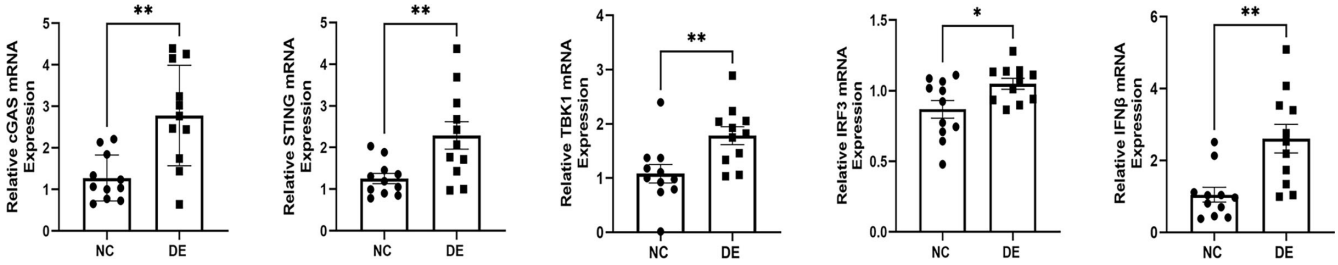

Figure 8. RT-qPCR results show the mRNA expression levels of cGAS, STING, TBK1, IRF, and IFN-β in the NC and DE groups ($n = 11$/group). The data are presented as mean ± SD. *$P < 0.05$, **$P < 0.01$.

chondrial DNA leaking into the cytoplasm, leading to STING translocation, resulting in the development of inflammation; and (3) inhibition of the cGAS-STING pathway dampens the increased expression of inflammatory factors. Targeting of the cGAS-STING pathway could be a new target for environmental DE therapy. However, further in-depth studies on the downstream targets and specific molecular regulatory mechanisms of the cGAS-STING pathway in environmental DE are warranted.

Acknowledgments

Supported by the National Natural Science Foundation of China (82371035&82171021) and Foundation of Wenzhou Science & Technology Bureau (Y2023177).

Disclosure: **X. Tan**, None; **Q. Chen**, None; **Z. Chen**, None; **Z. Sun**, None; **W. Chen**, None; **R. Wei**, None

References

1. Kamøy B, Magno M, Nøland ST, et al. Video display terminal use and dry eye: preventive measures and future perspectives. *Acta Ophthalmol*. 2022;100(7):723–739.
2. Pflugfelder SC, de Paiva CS. The pathophysiology of dry eye disease: what we know and future directions for research. *Ophthalmology*. 2017 Nov;124(11S):S4–S13.
3. Ren Y, Chen J, Zheng Q, et al. Short-term effect of a developed warming moist chamber goggle for video display terminal-associated dry eye. *BMC Ophthalmol*. 2018;18(1):33.
4. Zhang X, Chen Q, Chen W, et al. Tear dynamics and corneal confocal microscopy of subjects with mild self-reported office dry eye. *Ophthalmology*. 2011;118(5):902–907.
5. Perez VL, Stern ME, Pflugfelder SC. Inflammatory basis for dry eye disease flares. *Exp Eye Res*. 2020;201:108294.
6. Li S, Lu Z, Huang Y, et al. Anti-oxidative and anti-inflammatory micelles: break the dry eye vicious cycle. *Adv Sci (Weinh)*. 2022;9(17):e2200435.
7. Li DQ, Luo L, Chen Z, Kim HS, Song XJ, Pflugfelder SC. JNK and ERK MAP kinases mediate induction of IL-1β, TNF-α and IL-8 following hyperosmolar stress in human limbal epithelial cells. *Exp. Eye Res*. 2006;82:588–596.
8. Luo L, Li DQ, Doshi A, Farley W, Corrales RM, Pflugfelder SC. Experimental dry eye stimulates production of inflammatory cytokines and MMP-9 and activates MAPK signaling pathways on the ocular surface. *Invest Ophthalmol Vis Sci*. 2004;45(12):4293–4301.
9. Dogru M, Kojima T, Simsek C, Tsubota K. Potential role of oxidative stress in ocular surface inflammation and dry eye disease. *Invest Ophthalmol Vis Sci*. 2018;59(14):DES163–DES168.
10. Seen S, Tong L. Dry eye disease and oxidative stress. *Acta Ophthalmol*. 2018;96(4):e412–e420.
11. Barrera MJ, Aguilera S, Castro I, et al. Dysfunctional mitochondria as critical players in the inflammation of autoimmune diseases: potential role in Sjögren's syndrome. *Autoimmun Rev*. 2021;20(8):102867.
12. Chi W, Hua X, Chen X, et al. Mitochondrial DNA oxidation induces imbalanced activity of NLRP3/NLRP6 inflammasomes by activation of caspase-8 and BRCC36 in dry eye. *J Autoimmun*. 2017;80:65–76.
13. Picca A, Calvani R, Coelho-Junior HJ, Marzetti E. Cell death and inflammation: the role of mitochondria in health and disease. *Cells*. 2021;10(3):537.
14. Rodríguez-Nuevo A, Zorzano A. The sensing of mitochondrial DAMPs by non-immune cells. *Cell Stress*. 2019;3:195–207.
15. Barrera MJ, Aguilera S, Castro I, et al. Dysfunctional mitochondria as critical players in the inflammation of autoimmune diseases: potential role in Sjögren's syndrome. *Autoimmun Rev*. 2021;20(8):102867.
16. Alessandri C, Conti F, Pendolino M, Mancini R, Valesini G. New autoantigens in the antiphospholipid syndrome. *Autoimmun Rev*. 2011;10:609–616.
17. Kausar S, Yang L, Abbas MN, et al. Mitochondrial DNA: a key regulator of anti-microbial innate immunity. *Genes (Basel)*. 2020;11(1):86.
18. Motwani M, Pesiridis S, Fitzgerald KA. DNA sensing by the cGAS-STING pathway in health and disease. *Nat Rev Genet*. 2019;20:657–674.
19. Andreeva L, Hiller B, Kostrewa D, et al. cGAS senses long and HMGB/TFAM- bound U-turn DNA by forming protein-DNA ladders. *Nature*. 2017;549:394–398.
20. Willemsen J, Neuhoff MT, Hoyler T, et al. TNF leads to mtDNA release and cGAS/STING-dependent interferon responses that support inflammatory arthritis. *Cell Rep*. 2021;37(6):109977.
21. Liu Z, Wang M, Wang X, et al. XBP1 deficiency promotes hepatocyte pyroptosis by impairing mitophagy to activate mtDNA-cGAS-STING signaling in macrophages during acute liver injury. *Redox Biol*. 2022;52:102305.
22. Hu M, Zhou M, Bao X, et al. ATM inhibition enhances cancer immunotherapy by promoting mtDNA leakage and cGAS/STING activation. *J Clin Invest*. 2021;131(3):e139333.
23. Yu CH, Davidson S, Harapas CR, et al. TDP-43 triggers mitochondrial DNA release via mPTP to activate cGAS/STING in ALS. *Cell*. 2020;183(3):636–649.
24. Zhang X, Bai XC, Chen ZJ. Structures and mechanisms in the cGAS-STING innate immunity pathway. *Immunity*. 2020;53(1):43–53.
25. Decout A, Katz JD, Venkatraman S, Ablasser A. The cGAS-STING pathway as a therapeutic target in inflammatory diseases. *Nat Rev Immunol*. 2021;21(9):548–569.

26. Hopfner KP, Hornung V. Molecular mechanisms and cellular functions of cGAS-STING signalling. *Nat Rev Mol Cell Biol*. 2020;21(9):501–521.
27. Civril F, Deimling T, de Oliveira Mann CC, et al. Structural mechanism of cytosolic DNA sensing by cGAS. *Nature*. 2013;498(7454):332–337.
28. Shang G, Zhu D, Li N, et al. Crystal structures of STING protein reveal basis for recognition of cyclic di-GMP. *Nat Struct Mol Biol*. 2012;19(7):725–727.
29. Shu C, Yi G, Watts T, et al. Structure of STING bound to cyclic di-GMP reveals the mechanism of cyclic dinucleotide recognition by the immune system. *Nat Struct Mol Biol*. 2012;19(7):722–724.
30. Gao P, Ascano M, Zillinger T, et al. Structure-function analysis of STING activation by c[G(2′,5′)pA(3′,5′)p] and targeting by antiviral DMXAA. *Cell*. 2013;154:748–762.
31. Ergun SL, Fernandez D, Weiss TM, Li L. STING polymer structure reveals mechanisms for activation, hyperactivation, and inhibition. *Cell*. 2019;178(2):290–301.
32. Shang G, Zhang C, Chen ZJ, et al. Cryo-EM structures of STING reveal its mechanism of activation by cyclic GMP-AMP. *Nature*. 2019;567(7748):389–393.
33. Mukai K, Konno H, Akiba T, et al. Activation of STING requires palmitoylation at the Golgi. *Nat. Commun.* 2016;7:11932.
34. Zou M, Ke Q, Nie Q, et al. Inhibition of cGAS-STING by JQ1 alleviates oxidative stress-induced retina inflammation and degeneration. *Cell Death Differ*. 2022;29(9):1816–1833.
35. Han F, Guo H, Wang L, et al. The cGAS-STING signaling pathway contributes to the inflammatory response and autophagy in Aspergillus fumigatus keratitis. *Exp Eye Res*. 2021;202:108366.
36. Parker ZM, Murphy AA, Leib DA. Role of the DNA sensor STING in protection from lethal infection following corneal and intracerebral challenge with herpes simplex virus 1. *J Virol*. 2015;89(21):11080–11091.
37. Royer DJ, Carr DJ. A STING-dependent innate-sensing pathway mediates resistance to corneal HSV-1 infection via upregulation of the antiviral effector tetherin. *Mucosal Immunol*. 2016;9(4):1065–1075.
38. Ouyang W, Wang S, Yan D, et al. The cGAS-STING pathway-dependent sensing of mitochondrial DNA mediates ocular surface inflammation. *Signal Transduct Target Ther*. 2023;8(1):371.
39. Chen W, Zhang X, Zhang J, et al. A murine model of dry eye induced by an intelligently controlled environmental system. *Invest Ophthalmol Vis Sci*. 2008;49(4):1386–1391.
40. Tsubota K, Yokoi N, Watanabe H, et al. A new perspective on dry eye classification: proposal by the Asia Dry Eye Society. *Eye Contact Lens*. 2020;46(5):e39.
41. Guo Y, Gu R, Gan D, Hu F, Li G, Zu G. Mitochondrial DNA drives noncanonical inflammation activation via cGAS-STING signaling pathway in retinal microvascular endothelial cells. *Cell Commun Signal*. 2020;18(1):172.
42. Guo Y, Gan D, Hu F, et al. Intravitreal injection of mitochondrial DNA induces cell damage and retinal dysfunction in rats. *Biol Res*. 2022;55(1):22.
43. An J, Durcan L, Karr RM, et al. Expression of cyclic GMP-AMP synthase in patients with systemic lupus erythematosus. *Arthritis Rheumatol*. 2017;69(4):800–807.
44. Kato Y, Park J, Takamatsu H, et al. Apoptosis-derived membrane vesicles drive the cGAS-STING pathway and enhance type I IFN production in systemic lupus erythematosus. *Ann Rheum Dis*. 2018;77(10):1507–1515.
45. Thim-uam A, Prabakaran T, Tansakul M, et al. STING mediates lupus via the activation of conventional dendritic cell maturation and plasmacytoid dendritic cell differentiation. *iScience*. 2020;23:101530.
46. Wang J, Li R, Lin H, et al. Accumulation of cytosolic dsDNA contributes to fibroblast-like synoviocytes-mediated rheumatoid arthritis synovial inflammation. *Int Immunopharmacol*. 2019;76:105791.
47. Zheng Q, Ren Y, Reinach PS, et al. Reactive oxygen species activated NLRP3 inflammasomes initiate inflammation in hyperosmolarity stressed human corneal epithelial cells and environment-induced dry eye patients. *Exp Eye Res*. 2015;134:133–140.
48. Zheng Q, Ren Y, Reinach PS, et al. Reactive oxygen species activated NLRP3 inflammasomes prime environment-induced murine dry eye. *Exp Eye Res*. 2014;125:1–8.
49. Peng F, Jiang D, Xu W, et al. AMPK/MFF activation: role in mitochondrial fission and mitophagy in dry eye [published correction appears in *Invest Ophthalmol Vis Sci*. 2022;63(13):24]. *Invest Ophthalmol Vis Sci*. 2022;63(12):18.
50. Torre-Minguela C, Gómez AI, Couillin I, Pelegrín P. Gasdermins mediate cellular release of mitochondrial DNA during pyroptosis and apoptosis. *FASEB J*. 2021;35(8):e21757.
51. McKeage MJ, Reck M, Jameson MB, et al. Phase II study of ASA404 (vadimezan, 5,6-dimethylxanthenone-4-acetic acid/DMXAA) 1800mg/m (2) combined with carboplatin and paclitaxel in previously untreated advanced non-small cell lung cancer. *Lung Cancer*. 2009;65:192–197.
52. Wang Z, Celis E. STING activator c-di-GMP enhances the anti-tumor effects of peptide vaccines in melanoma-bearing mice. *Cancer Immunol Immunother*. 2015;64:1057–1066.
53. Chinook Therapeutics, Inc. (formerly Aduro). A phase I, open label, multicenter study of the safety and efficacy of MIW815 (ADU-S100) administered by intratumoral injection to patients with advanced/metastatic solid tumors or lymphomas. 2021, https://clinicaltrials.gov/study/NCT02675439. Accessed September 8, 2023.
54. Merck Sharp & Dohme LLC. Phase 1 open-label, multicenter study of MK-1454 administered by intratumoral injection as monotherapy and in combination with pembrolizumab for patients with advanced/metastatic solid tumors or lymphomas. 2022, https://clinicaltrials.gov/study/NCT03010176. Accessed September 8, 2023.
55. GlaxoSmithKline. A phase I first time in human open label study of GSK3745417 administered with and without anticancer agents in participants with advanced solid tumors. 2023, https://clinicaltrials.gov/study/NCT03843359. Accessed September 8, 2023.
56. Eisai Inc. An open-label, multicenter phase 1/1b study of intratumorally administered STING agonist E7766 in subjects with advanced solid tumors or lymphomas—INSTAL-101. 2023, https://clinicaltrials.gov/study/NCT04144140. Accessed September 8, 2023.
57. Tian X, Liu C, Wang Z, et al. The induction of inflammation by the cGAS-STING pathway in human dental pulp cells: a laboratory investigation. *Int Endod J*. 2022;55(1):54–63.
58. Wu B, Xu MM, Fan C, et al. STING inhibitor ameliorates LPS-induced ALI by preventing vascular endothelial cells-mediated immune cells chemotaxis and adhesion. *Acta Pharmacol Sin*. 2022;43(8):2055–2066.
59. Gui X, Yang H, Li T, et al. Autophagy induction via STING trafficking is a primordial function of the cGAS pathway. *Nature*. 2019;567(7747):262–266.
60. Li Y, Chen H, Yang Q, et al. Increased Drp1 promotes autophagy and ESCC progression by mtDNA stress mediated cGAS-STING pathway. *J Exp Clin Cancer Res*. 2022;41(1):76.
61. Peng Y, Wu X, Zhang S, et al. The potential roles of type I interferon activated neutrophils and neutrophil extracellular traps (NETs) in the pathogenesis of primary Sjögren's syndrome. *Arthritis Res Ther*. 2022;24(1):170.